

## EVALUATION OF TWO-WAY SHAPE MEMORY EFFECT IN BI-LAYER NITI THIN FILM

Mahmoud Nili-Ahmadabadi<sup>1,2</sup>, Maryam Mohri<sup>1</sup>

<sup>1</sup>*School of Metallurgy and Materials Engineering, College of Engineering, University of Tehran, Tehran, Iran.*

<sup>2</sup>*Center of Excellence for High Performance Materials, University of Tehran, Tehran, Iran.*

### Abstract

One bi-layer Ni-Ti thin films with chemical compositions of Ni<sub>45</sub>TiCu<sub>5</sub> /Ni<sub>50.8</sub>Ti (numbers indicate at.%) determined by energy dispersive X-ray spectroscopy was deposited on Si substrates using RF magnetron sputtering. The structures and transformation temperatures of annealed thin films at 773 K for 1h were studied using grazing incidence X-ray diffraction (GIXRD) and differential scanning calorimetry (DSC), respectively. Nanoindentation was used to characterize the mechanical properties. The DSC and X-ray diffraction results indicated the bi-layer was composed of austenitic and martensitic thin films. The bi-layer thin film exhibited a combined pseudo elastic behavior and shape memory effect at the same time similar to the austenitic and martensitic thin films, respectively. The combination of pseudo elastic with shape memory effect produces a two-way shape memory effect with a reduced hysteresis in the bi-layers.

**Key words:** NiTi bi-layer thin film, Pseudo elastic, Two-way Shape memory effect

### 1. INTRODUCTION

NiTi alloys as a shape memory alloys (SMAs) are attractive for a wide range of smart designs and advanced applications owing to their excellent functional properties, including shape memory effect and pseudo elasticity [1–3]. Advanced engineering applications create a demand for development of novel structured TiNi. NiTi thin films are manufactured to suit the dimensional requirements in micro-electro-mechanical systems (MEMSs) [4,5]. The functional properties of SMAs are often noticed in two distinctive behaviors, known as pseudo elasticity and the shape memory effect [6]. The weak controllability of the shape memory element is a challenge for actuator design. One way to solve this problem is to create functionally graded NiTi components [7,8].

The two-way shape memory effect is highly desirable in the manufacture of the MEMS [9]. Controlling the transformation of Ni-Ti thin films are achieved by changing the composition and microstructure of a single homogeneous layer [10, 11]. Previous studies have indicated that SMA thin films with compositional gradients have the added feature of an intrinsic two-way shape memory effect (TWSME) [12-13]. In order to successfully develop functionally graded TiNi thin films for MEMS application, it is necessary to characterize and control the variations in composition, thermo-mechanical properties and residual stress in these films [7, 14]. While the potential applications for shape memory alloys (SMAs) in MEMS are large, the difficulties with fabricating quality material and achieving TWSME are preventing widespread use of this actuator material.

The paper aims to design and prepare bi-layer thin film with a gradient in chemical composition. Special attention has been paid to the shape memory behavior and super elasticity effect of the bi-layer with different chemical compositions. In addition, it has been shown the bi-layer NiTi films can be fabricated with a two-way shape memory effect without complicated heat treatment and training process that is incompatible with MEMS processing.

## 2. MATERIAL AND METHODS

One bi-layer thin film ( $\text{Ni}_{45}\text{TiCu}_5/\text{Ni}_{50.8}\text{Ti}$ ), has been deposited on Si (111) substrate using RF magnetron sputtering system using two alloy NiTi and NiTiCu targets. Due to the different angular sputtering distributions for Ni and Ti, the film composition deviates from the composition of the target. A typical loss rate of 4-4.5 at% Ti between cast-melted target and sputter deposited film was reported [15]. In order to compensate for Ti loss, the Ti concentration of the targets is about 54 at%. The deposition parameters are shown in Table 1.

**Table 1** Sputtering parameters

<b>Base pressure</b>	$<10^{-7}$ mbar
<b>Ar gas pressure</b>	$3 \times 10^{-3}$ mbar
<b>Target substrate distance</b>	50 mm
<b>Target power (NiTi target)</b>	150 W
<b>Thickness of each layer</b>	$\approx 600$ nm
<b>Deposition temperature</b>	Room temperature

The substrate holder was kept rotating during deposition in order to achieve a uniform distribution of composition. The film thicknesses were determined using a Dektak surface profile. The compositions of the as-deposited single layer thin films were determined by energy dispersive X-ray analysis (EDXA). In order to crystallize the as-deposited thin film, it were annealed at 773 K for 1h under vacuum ( $<10^{-7}$  mbar). The crystallization and phase transformation temperatures were measured using DSC (NETZSCH DSC 404C) on the thin film after removal from the substrates. Heating and cooling rates were maintained at 10°C/min.

Grazing incidence X-ray diffraction measurements of the as-deposited and crystallized thin films were carried out at room temperature by using a Bruker diffractometer of Cu-K $\alpha$  radiation. The film surface morphology was studied using tapping mode atomic force microscopy (AFM: Digital Instruments Nanoscope III). AFM was also used to image the residual indent to determine the extent of pile-up or sink in and the recovery of the indent effect after heating.

The annealed thin films were then subjected to mechanical analysis by means of nanoindentation using an Agilent G200-DCM Nanoindenter equipped with a Berkovich diamond indenter. The maximum indentation load was 5 mN. Both load and displacement were recorded during the entire loading and unloading cycle. The indenter was loaded at a constant indentation strain rate of 0.025 s<sup>-1</sup> to the maximum load and the load was held constant for 10s. Then, the specimens were unloaded to 10% of maximum load and the load was held constant for 60s, while the displacement was monitored to determine the displacement rate produced by thermal expansion in the system. Finally, the sample was unloaded completely. The displacement data were corrected assuming a constant drift rate throughout one indentation test. The load-displacement experiments were repeated at five different locations on the surface of the films. Through the use of nanoindentation and atomic force microscopy (AFM) methods the shape memory effect is observed in the nanoscale regime. After the nanoindentation tests, the indents were scanned using an AFM and then the samples were heated up to  $A_f$  (austenite finish temperature)  $\approx 353$  K for 2 min and then were allowed to cool. This process transformed the martensite to austenite which in turn the shape memory effect (SME) occurs. The films were scanned using the AFM, and the indents imaged again. The change in the depth of the remnant indentations due to the shape memory effect was quantified using NanoScope Analysis software.

### 3. RESULT AND DISCUSSION

#### 3.1. Structural analysis

The as-deposited thin film structure was studied using GIXRD. The X-ray pattern of the as-deposited thin film display a broad peak around  $2\theta \approx 43^\circ$  (Fig.1) which indicated that the as-deposited thin films are in amorphous state (Fig.1). In general, the film deposited at room temperature was usually amorphous in nature. The amorphous NiTi thin films do not exhibit the shape memory effect, and then an annealing process is necessary to yield the shape memory effect and super elasticity behaviors. Therefore, high temperature deposition or post annealing was required to make them crystalline. Fig.2 gives typical continuous heating DSC trace obtained from the thin film. The DSC traces exhibits two exothermic crystallization peaks which related to each layer in the thin films. As Chang and Grummon [16] showed, the crystallization temperature of NiTi thin films at a heating rate of  $10^\circ\text{C}/\text{min}$  decreased with increasing the Ti content, from 763 K for  $\text{Ni}_{52.6}\text{Ti}_{47.4}$  to 748 K for  $\text{Ni}_{49}\text{Ti}_{51}$ . As illustrated in Fig.2, the onset crystallization temperature and peak temperature decreases with reduced Ni contents. The peaks at 736 K and 760 K are related to the Ti-rich and Ni-rich layers, respectively. In the other words, the Ni-rich layer is more stable than the Ti-rich layer during crystallization annealing. Therefore, it means that the chemical compositions have significant influences on thermal stability in NiTi alloy thin films. According to the DSC results, the bi-layer thin film was crystallized at 773 K for 1h. The XRD pattern of the crystallized thin film presented in Fig.1. The austenite, martensite and R-phase are present in the bi-layer thin film. The presence of R-phase, suggests that a multi-step transformation ( $\text{B2} \leftrightarrow \text{R}$ ,  $\text{B2} \leftrightarrow \text{B19}'$ ,  $\text{R} \leftrightarrow \text{B19}'$ ) happened in the thin film. This multi-step transformation was confirmed by DSC measurement (Fig.3).

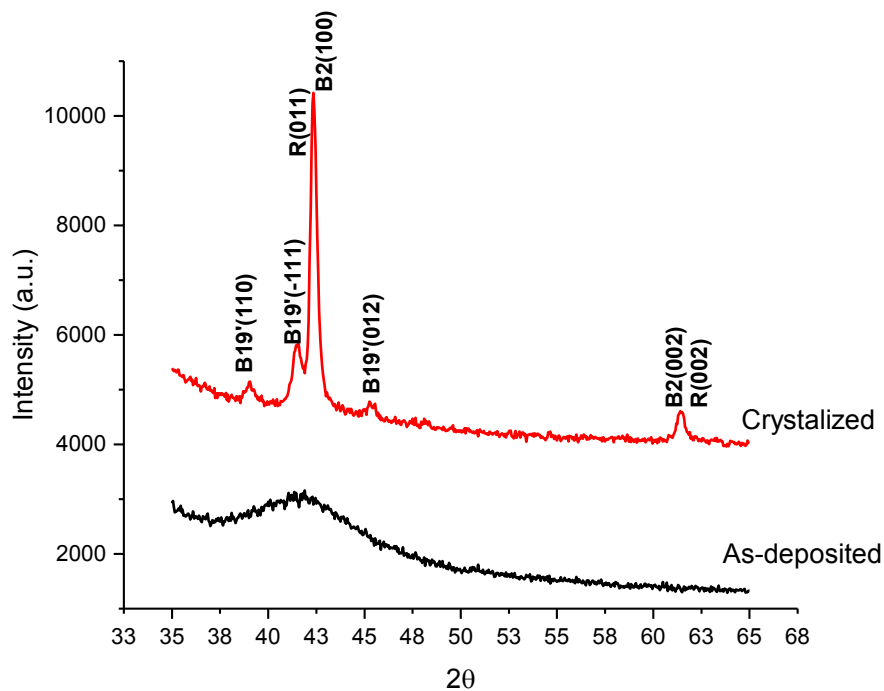


**Fig. 1** XRD profile of the bi-layer thin film before and after annealing at 773 K for 1h.

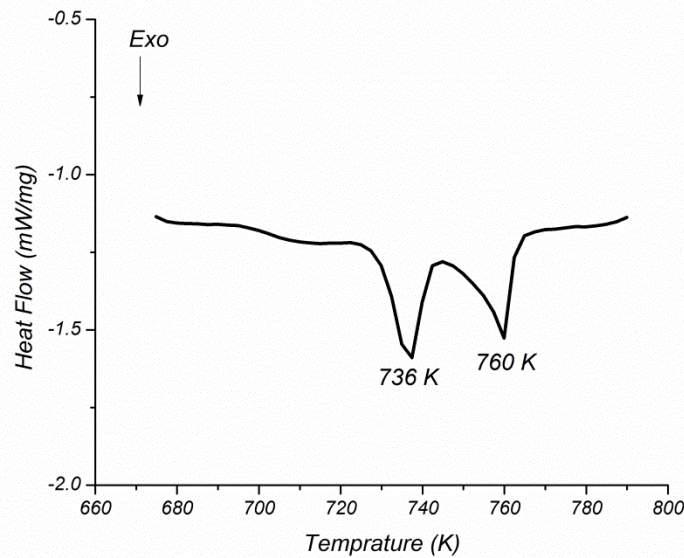


**Fig. 2** DSC curve of crystallization temperature of the as deposited bi-layer thin film.

DSC curves of the bi-layer thin film illustrate two transformation zones associated with the each layer transformation during thermal cycling. In the heating curve, the first peak is related to the transformation of martensite to the austenite phase in the Ni-rich layer and the second peak shows multiple step phase transformation ( $B19' \rightarrow R$ ,  $B19' \rightarrow B2$ ,  $R \rightarrow B2$ ) related to the TiNiCu layer. Reverse transformations occurred in the cooling curve are shown in Fig.3. The small difference between the peak temperatures upon heating and cooling also known as a narrow temperature hysteresis could be related to the occurrence of a R-phase transitions in the bi-layer. Because of the narrow hysteresis width, NiTi films which exhibit the intermediate R-phase transition are of interest for MEMS applications. The small hysteresis enables the fabrication of higher-speed actuators as well as of regulated actuators without the need for a complex control algorithm [15].

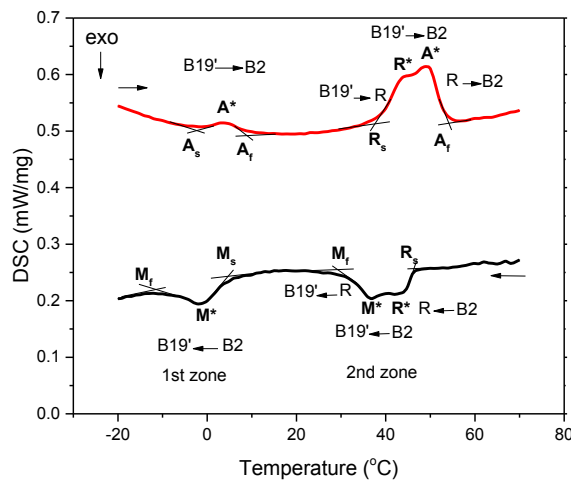


**Figure 3.** DSC curves of the bi-layer after annealing at the 773 K for 1h, 1<sup>st</sup> zone is related to austenitic layer and 2<sup>nd</sup> zone is related to martensitic layer.

### 3.2. Mechanical properties

For evaluation of mechanical properties of the NiTi thin films, load-displacement curves of the annealed bi-layer thin film obtained from the nanoindentation are shown in Fig.4. All the indentation tests were carried out in air at room temperature and relative humidity of 50%. The elastic recovery of the bi-layer is more complex than the single-layer thin films during the nanoindentation, due to the influences of the interface between the layers and composition gradient across the film thickness. It is expected that the diffusion during annealing reduces the level of residual stress at the interface [17]. The indentation induced super elasticity effect can be characterized by the depth recovery ratio ( $\mu$ ) of the load-displacement curves by using the following equation [17]:

$$\text{Depth Recovery Ratio } (\mu) = (h_{\max} - h_r) / h_{\max} \quad (1)$$

where  $h_{\max}$  is the penetration depth at the maximum load and  $h_r$  is the depth when the load returns to zero during unloading. The depth recovery ratio of the bi-layer thin film is 0.44.

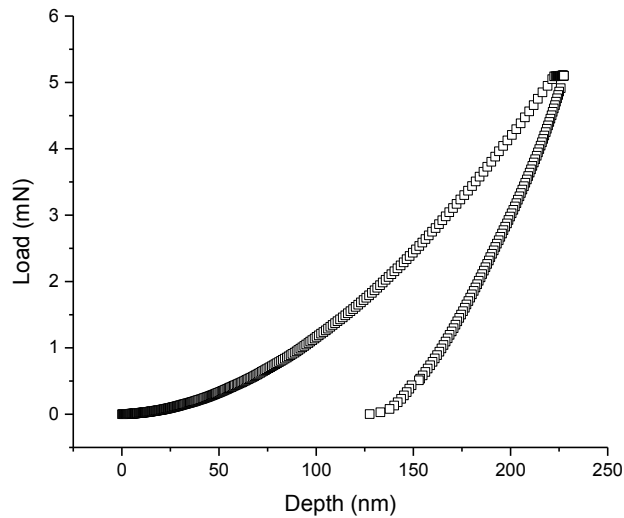


**Fig. 4.** The load-depth curve of the bi-layer thin film.

The processes occurring during indentation in the martensitic and austenitic structures in NiTi alloys can be explained by Johnson's spherical cavity model [18-19]. According to this model, the deformation of the solid under the indenter tip occurs by plastic deformation in the region nearest to the tip where stresses are greatest, followed by martensite-twin rearrangement in the case of a martensitic structure or stress-induced martensitic (SIM) transformation (pseudo elasticity) in the case of austenitic structure, and finally elastic deformation in the region far from the tip. Although these regions are not sharply specified, but by using the modified spherical cavity model, the phase transformation-elastic boundary radius can be located such that:

$$C = \frac{d}{\tan\beta} \left[ \frac{E \tan\beta}{6Y(1-\nu)} + \frac{2-4\nu}{3-2\nu} \right]^{1/3} \quad (2)$$

where  $C$  is an phase transformation-elastic boundary,  $d$  is indentation depth,  $\beta$  is the angle between the surface and indenter ( $24.65^\circ$  for a Berkovich indenter),  $E$  is Young's modulus,  $Y$  is yield stress of the material ( $Y_{\text{Martensite}}=0.2\text{GPa}$  (the critical stress for martensite-twin reorientation),  $Y_{\text{Austenite}}=0.6\text{GPa}$  (the critical stress for stress-induced martensitic transformation (pseudo elasticity))) [20-21] and  $\nu$  is Poisson's ratio (0.33 for NiTi alloy).

In the bi-layer, the NiTiCu upper layer is martensitic while in the bottom Ni-rich layer an austenitic structure is dominant. There is no significant recovery in the unloading curve indicating more predominantly de-twinning and plastic deformation in the martensitic upper layer. Because of the using Berkovich indenter tip, plastic deformation is introduced in the material. In the austenite structures, stress induced martensite transformation (SIM) and de-twinning can occur, while in the martensitic phase, only de-twinning takes place. Martensite formation in the austenitic phase out of the plastic deformation zone is metastable, and thus reverses on unloading, leading to recoverable strain, while de-twinning results in the martensitic structures are permanent deformation, unless a subsequent heating step is included [22].

According to Eq. (2) and calculated (C), by increasing the depth of the indentation, the radius of the transformed region (C) is more than the upper layer thickness. Hence, the bottom layer contributes to the deformation. In the bi-layer because of the high indentation depth, the bottom austenitic layer has participated in the recovery process.

In addition to the shape memory properties derived from the indentation load-displacement curves, further characterization of the films can be achieved through a coupled nanoindentation -AFM experiment. The recovered depth of indentation is a measure of the available shape memory material within the film. Residual indentation depth in martensitic film can be caused to recover through the shape memory effect by heating the film above their austenitic finish temperature ( $A_F$ ). Measurements of the indentation depths before and after heating are used to calculate the depth recovery ratio for films. This recovery can be quantified using a recovery ratio:

$$R = \frac{D_{bh} - D_{ah}}{D_{bh}} \quad (3)$$

where  $D_{bh}$  and  $D_{ah}$  are indent depth before and after heating, respectively. The insets in Fig.5 show profiles of the indentations before and after heating which were used to determine  $D_{bh}$  and  $D_{ah}$ , respectively. In the bi-layer after heating, the indent becomes shallower, which indicates recovery of the deformation accommodated through shape memory process. The recovery ratio (R) of the bi-layer thin film is 0.31.

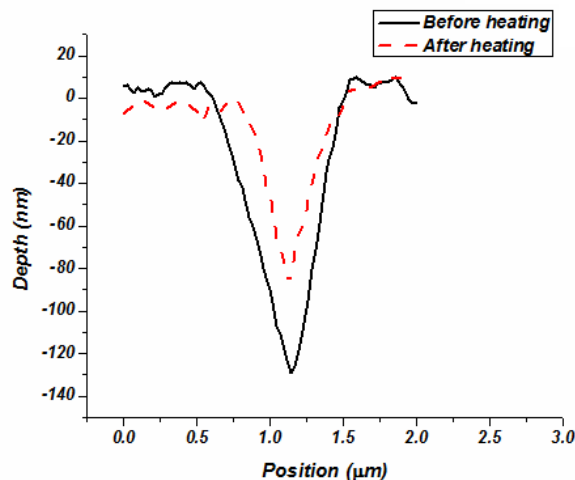


**Fig. 5.** Cross-section of AFM scan of indentation in the bi-layer thin film before and after heating showing depth recovery. Films annealed at 353 K for 2 min.

For studying the two-way shape memory effect of the bi-layer thin film, freestanding film was heated to above 353 K and then cooled to room temperature. The two-way shape memory effect can be clearly observed from the photos of freestanding bi-layer thin film as shown in Fig.6. At room temperature, the film rolls due to the existence of residual stress as shown in Fig.6(a). When heated gradually above  $A_r$ , it can be seen that the film is gradually unrolled as shown from Fig.6(b), due to the shape memory effect. After cooling down to room temperature, the sample rolls again, i.e. recovering to its room temperature shape as shown in Fig.6(c). This two-way shape memory effect is not generated by the usual special thermo-mechanical training procedures of Ni-Ti thin films, and it is most likely due to the residual stress in the bi-layer thin film structure. The integration of pseudo elastic with shape memory characteristics produces a two-way shape memory, because variations in the residual stress in thickness direction will enable a biasing force to build up inside the thin film. The residual stresses that are larger than the yield stress of the martensite phase can bend a film into a rolled-shape while the austenitic layer is in elastic or pseudo elastic state, but when heated the martensitic layer transformed to the austenite phase and can overcome the residual stress and reverts to unrolled-shape. After subsequent cooling because of the transformation austenite to the martensite and residual stress, the multilayer rolled again. Then, the combination of pseudo elastic with shape memory effect produces a two-way shape memory. Maximum force output utilizing the two-way effect is dependent on the magnitude of the residual stresses. In other word the force available during recovery to the low temperature phase supplied by the residual stresses, while in heating it is the force of the shape memory effect after overcoming the opposing residual stresses. This two-way shape memory effect is quite applicable, to develop thin film micro-actuators.

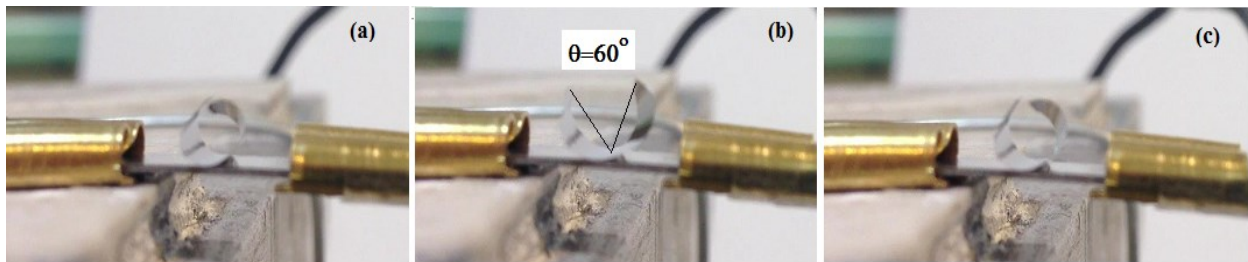


**Fig. 6.** Demonstration of the two-way shape memory effect of the bi-layer thin film. The film changes spontaneously between (a) room temperature shape, (b) high temperature shape and (c) room temperature shape.

## CONCLUSIONS

The experimental results led to the development of a graded bi-layer NiTi thin films ( $Ni_{45}TiCu_5/Ni_{50.8}Ti$ ) which show the shape memory effect and pseudo elastic behavior. These behaviors reflect on the experimental results and can be interpreted by X-ray diffraction, DSC measurement and mechanical properties presented in this paper. The austenite, martensite and R-phase are present in the bi-layer thin film and the bi-layer thin film exhibit a multi-step transformation  $B2 \leftrightarrow R$ ,  $B2 \leftrightarrow B19'$ ,  $R \leftrightarrow B19'$  during thermal cycling. Nanoindentation studies revealed that the bi-layer thin film exhibited a combined pseudo elastic behavior and shape memory effect which lead to show intrinsic two-way shape memory effect.

## REFERENCES:

- [1] L. Delaey, R.V. Krishnan, H.Tas; *J. Mater. Sci.*, 1974, vol.9, pp.1521-1535.
- [2] S. Miyazaki, K. Otsuka, C.M.Wayman,; *Acta Metall.*, 1989, vol.37, pp.1885-1890.
- [3] Y. Liu, P.G. McCormick,; *Acta Metal. Mater.*, 1990, vol.38, pp.1321-1326.
- [4] Y. Fu, W. Huang, H. Du, X. Huang, J.Tan, X. Gao,; *Surf. Coat. Technol.*, 2001, vol.145, pp.107-111.

- 
- [5] T. Shahrabi, S.Sanjabi, E. Saebnoori, Z.H. Barber,: *Mater. Lett.*, 2008, vol.62, pp.2791-2794.
- [6] L. Sun, W.M.Huang, Z. Ding, Y.Zhao, C.C. Wang, H. Purnawali,: *Mater. Des.*, 2012, vol.33, pp.577-640.
- [7] S. Miyazaki, Y.Q. Fu, W.M. Huang, *Overview of sputter-deposited Ti-Ni based thin films*. In: S. Miyazaki, Y.Q. Fu, W.M. Huang, editors. *Thin film shape memory alloys: fundamentals and device applications*. (Cambridge: Cambridge University Press, 2009, p. 48.
- [8] B.Winzek, S. Schmitz, H. Rumpf, T. Sterzl, R. Hassdorf, S. Thienhaus, *Mater. Sci. Eng. A*, 2004, vol.378, pp.40-46.
- [9] P. Chan, C. Chung and K. Ng, *J. Alloys Compd.* 2008, vol.449, 148-151.
- [10] G. Airoldi, A. Corsi and G. Riva, *Mater. Sci. Eng. A* 1998, vol.241, 233-240.
- [11] A. Gyobu, Y. Kawamura, T. Saburi and M. Asai, *Mater. Sci. Eng. A* 2001, vol.312, 227-231.
- [12] D. Cole, *Fabrication and Characterization of Compositionally graded Shape Memory Alloy Films*, Maryland: Phd thesis, University of Maryland, 2009.
- [13] R. Martins, N. Schell, A. Mücklich, H. Reuther and M. Beckers, *Appl. Phys. A*, 2008, vol.91, 291-299.
- [14] K. Ho and G. Carman, *Thin Solid Films*, 2000, vol.370, 18-29.
- [15] H.C. Ling, R. Kaplow,: *Metall. Trans. A*, 1980, vol.11, pp.77-83.
- [16] L. Chang, D.S.Grummon: *Phil. Mag. A*, 1997, vol.76, pp.191-219.
- [17] L. Qian, M. Li, Z. Zhou, H. Yang, X. Shi,: *Surf. Coat. Technol.*, 2005, vol.195, pp.264-271.
- [18] K.L. Johnson, *Contact Mechanics*, (Cambridge : Cambridge University Press,1994).
- [19] G. Shaw, D. S. Stone, A. D. Johnson, A. B. Ellis and W.C. Crone,: *Appl. Phys. Lett.*, 2003, vol.83, pp.257-259.
- [20] A. Ishida, A. Takei, M. Sato, S. Miyazaki,: *Thin Solid Films*. 1996, vol.281-282, pp.337-339.
- [21] A. Ishida, M. Sato, T. Kimura and S. Miyazaki,: *Philos. Mag. A*, 2000, vol.80, pp.967-980.
- [22] K. Ho, G. Carman,: *Thin Solid Films*,. 2000, vol.370, pp.18-29.